Evaluating cubic equations of state for predictions of solid-fluid equilibrium in liquefied natural gas production

Xiaoxian Yang, Darren Rowland, Catherine C. Sampson, Peter E. Falloon, Eric F. May*

[1]*Fluid Science & Resources Division, Department of Engineering, University of Western Australia, Perth, Australia*

to be submitted to *Applied Energy* (2021)

Abstract

Solid formation and deposition in liquefied natural gas (LNG) production is a process hazard avoidable by careful determination of impurity solubility in the process stream. Accurate freeze-out predictions for LNG require robust thermodynamic models tuned to high-quality experimental data. Cubic equations of state (EoS) can be used to calculate solid-fluid equilibria (SFE) for LNG-relevant binary mixtures with the necessary accuracy, while retaining the computational efficiency ideal for process simulations. A comprehensive literature survey of the available experimental SFE data of LNG-relevant binary mixtures was carried out and used to determine the optimal binary interaction parameters for a range of commonly-used cubic EoS. Overall the, Peng-Robinson (PR) EoS performed best representing the SFE temperatures with a standard uncertainty of less than 2 K for most of the examined mixtures; the Soave-Redlich-Kwong (SRK), Peng-Robinson-Stryjek-Vera (PRSV) and Patel-Teja-Valderrama (PTV) equations produced similar results. The solubility of various impurities in methane was investigated with the optimized EoS across a range of temperature, and various retrograde behaviors were examined. The EoS models and the best-fit parameters obtained in this work have been incorporated into the *ThermoFAST* desktop application and a new free online implementation *ThermoFAST Web*.

Keywords: cubic equation of state, liquefied natural gas, solid fluid equilibrium

*Corresponding author. *Email address:* eric.may@uwa.edu.au.

1. Introduction

Natural gas can be liquefied to facilitate the large-scale non-pressurized storage and transport needed for its trans-oceanic trade. Currently, liquefied natural gas (LNG) trade accounts for approximately 33 % of the world's natural gas trade and is expected to increase substantially in coming years [1]. Freeze-out and deposition of solids within process equipment are, however, major challenges to LNG production and transportation [2]. In the event that freeze-out causes a blockage of the liquefaction train, the resultant process shutdown can lead to significant financial loss [3]. From average estimates of the current market value of LNG and LNG tanker capacity, an unplanned shutdown could cost approximately 25 million USD per missed shipment in cargo value alone [4, 5].

The issue of solids formation is generally addressed by over-engineered equipment operating specifications based on very conservative estimates of freeze-out potential. This approach reflects the lack of effective process modeling capability to predict solidification in LNG mixtures. To optimize equipment design and operation, process simulators must be based on robust and reliable thermodynamic property models capable of accurate solid-fluid equilibrium (SFE) predictions.

Cubic equations of state (EoS) have been used to predict fluid phase equilibria for over 100 years; as a result, pure fluid parameters for different cubic EoS are generally available from a variety of sources. To perform thermodynamic calculations for fluid mixtures, a cubic EoS must be combined with mixing rules, which account for the interactions between molecules of different species. In a mixing rule it is common to have at least one adjustable binary interaction parameter, which can be tuned to experimental data of binary mixtures to improve the accuracy of the EoS calculation. This tuning strategy has, along with the strong theoretical basis and simplicity of the models, made cubic EoS the dominant choice for modeling the phase equilibria of fluids in industrial software.

Adopting a similar methodology to Li and Yan [6], who evaluated five cubic EoS for liquid-vapor equilibrium (LVE) calculations of CO_2 and CO_2-mixtures in the area of carbon capture and storage, this work evaluates six cubic EOS for SFE calculations of binary methane mixtures in LNG processing. Methane is the primary component of LNG, with small amounts of nitrogen, ethane, propane, and butane, as well as trace quantities of water, carbon dioxide, pentane, benzene, cyclohexane and other heavy hydrocarbons [7-9]. Since methane is the dominant component, solid formation in LNG can be investigated by studying the SFE of key binary methane mixtures. Therefore, this work focuses on binary mixtures of methane with carbon dioxide, benzene, toluene, *n*-butane, *n*-pentane, neopentane, *n*-hexane, *n*-heptane and cyclohexane. Water is excluded from the current study as the phase equilibrium models needed to describe clathrate hydrates are qualitatively different from the SFE that occurs with the other compounds, in which the solid phase is a pure substance [10-12].

The six cubic EoS studied in this work are: Peng-Robinson (PR) [13], Soave-Redlich-Kwong (SRK) [14], Peng-Robinson-Stryjek-Vera (PRSV) [15], Wilson-Redlich-Kwong (WRK) [16], Patel-Teja-Valderrama (PTV) [17] and Redlich-Kwong (RK) [18]. The PR, SRK, PTV and RK EoS are widely used in gas industries, features of which have been described by Li and Yan [6]. The WRK EoS is a less-popular variant of SRK; both are modifications of the RK model. The PRSV EoS is a modification of PR with an extra fluid-specific parameter and is implemented within the Aspen process-design software package [19]. In this work, each cubic EoS is combined with the van der Waals mixing rules and a pure-solid fugacity model [20] to carry out SFE calculations. The results were compared with experimental SFE data taken from a comprehensive literature survey for methane binary mixtures; the most reliable SFE data were then utilized to fit the binary interaction parameters of each selected cubic EoS for each binary system.

The EoS models and their best-fit parameters obtained in this work have been incorporated into the *ThermoFAST* software package [21]. ThermoFAST uses a generalized cubic EoS coupled with a pure-solid fugacity calculation to provide rapid and robust thermodynamic calculations across all phases [22] and has been endorsed by the Gas Processors Association (GPA Midstream Association) as a preferred software package for SFE calculations in cryogenic natural gas processes. ThermoFAST is currently available in two forms: a free stand-alone desktop application [21] (which can be downloaded from www.fsr.ecm.uwa.edu.au/software/thermofast/), and a free web application ThermoFAST Web [23] (available online at thermofastweb.azurewebsites.net).

2. Literature Data Survey

A comprehensive literature survey of available experimental SFE data for LNG-relevant binary mixtures was carried out. The hydrocarbons selected for inclusion in the survey include the alkanes, cyclohexane, neopentane, benzene, toluene, ethylbenzene and the xylenes (*ortho*, *meta*, *para*). The cryogenic solvent fluids are composed predominantly of light hydrocarbons including methane, ethane, propane and n-butane. The data were collated and tabulated within the Joint Expert Speciation System (JESS) Hydrocarbon Solubility Database [24]. This computerized database contains over 1600 experimental solubility data for cryogenic hydrocarbon systems gathered from 48 sources published between 1896 and 2019 [25]. The database is also freely available online through the following link: http://jess.murdoch.edu.au/cryobase.shtml.

A summary of the available experimental SFE data for methane binary mixtures containing the solutes chosen for further study in this work is provided in Table 1. Figure 1 compares the total number of available data points for each system to the number of data points used for tuning (see

Section 4.3). Evaluation of the data sets is important to ensure that the experimental data used for tuning the cubic EoS are of sufficient quality. The JESS database [24] includes recommendations for selecting the highest quality data. This involves a weighting system in which each data point was assigned a value based on a variety of experimental factors and comparisons with available models [25]. The elimination of unreliable data in this work was based on the recommendations of JESS and then extended by comparison of the data with all six cubic EoS (see Section 4.2).

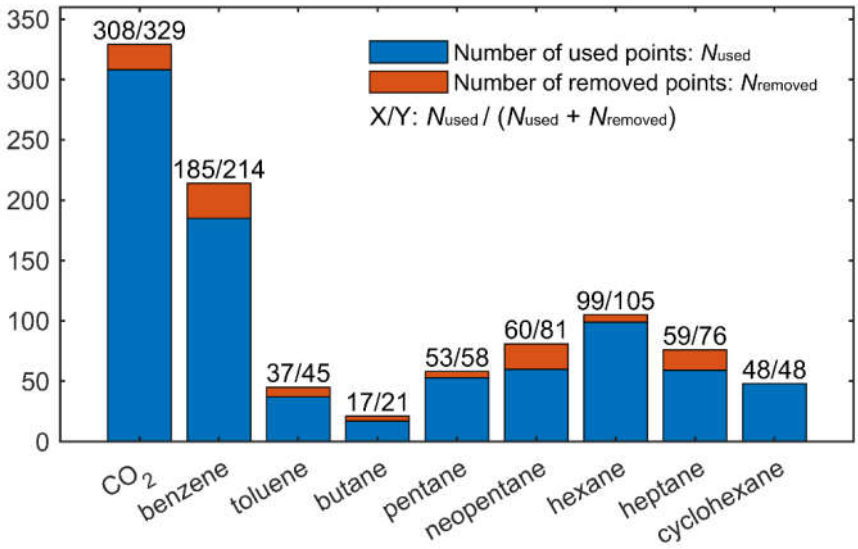

Figure 1. Total available, used, and removed experimental SFE data points in the determination of the best-fit binary interaction parameter between the solute component and methane.

Two challenges were frequently encountered while interpreting the data from literature. First, pressure information was not reported in some data sets measured under solid-liquid equilibrium (SLE) conditions. These data are identified in Table 1 by the value “none” in the pressure column. This issue originates from the assumption that the SLE condition is insensitive to pressure, which is not always valid. For example, the solubility of benzene in methane increases significantly at high pressures (higher than 40 MPa, see Section 4.5). The second challenge was that the data in

the source literature were reported with no (or incorrect) information provided regarding which type of equilibrium condition was measured. This could significantly impact the evaluation of data quality; an experimental value mistakenly labeled SLE that in fact was measured under a solid-liquid-vapor equilibrium (SLVE) condition would deviate from a calculated SLE curve by an amount potentially enough to make it classified as a low-quality data point. To prevent data from inadvertently being marked as low-quality due to an incorrect equilibrium condition assignment, a point-by-point analysis of each data set was undertaken to ensure the correct equilibrium condition was assigned to each point. To avoid such ambiguities, we highly recommend that all future experimental SFE data be provided with full information including temperature, pressure, composition and the equilibrium condition.

Another important piece of information that needs to be considered when interpreting literature data is the method of solvent composition determination. Experimental phase equilibria techniques can be broadly divided into two categories: analytical and synthetic methods [26, 27]. Analytical methods involve the compositional analysis of the equilibrium phases, with uncertainties arising from both the sampling method and detector calibration. In a synthetic measurement, the equilibrium composition in the bulk phase is assumed to be the overall mixture composition, with the inherent assumption that the solid at formation is negligible compared to the bulk mixture composition; this carries some associated compositional uncertainty. Knowing the basis used for determining composition helps to judge whether the reported composition could positively or negatively deviate from the real composition.

The literature review identified gaps in the available experimental data. As shown in Figure 1, fewer than 100 data points were available for binary mixtures of methane with pentane, hexane, toluene, butane, neopentane heptane and cyclohexane. For the latter five compounds listed, four

or fewer sources comprise all available data (see Table 1). There are considerably more data (329 values) for the methane + carbon dioxide binary mixture; however, no data are reported for mixtures with carbon dioxide content less than 100 ppm (parts-per-million), although carbon dioxide content in LNG is typically on the order of 50 ppm [28]. Unless otherwise stated, the unit for composition in this work is the mole fraction, and ppm notations are in molar basis. About 200 experimental values for the methane and benzene mixture are available, but the concentrations relevant to LNG processing (<0.01 mole fraction) are underrepresented.

Knobby

Fl		/K			/cm^3·mol^{-1}
meth		90.675	9284	9.757	2.492
car			3	13.802	8.583
be		78.674		1.337	10.41
to		78.000		027	5.827
n		134.895			9.17
n		143.470			16.51
ne		256.600			35
n-h		177.830			
n-he		182.550			
cyclo		279.860			

[a] Values OP 10.0 [6
database [70] for carbon
the remaining st

Table 3. Summary of the

EoS	Ω_a	Ω_b	
PR	0.45724	0.07779	$(1-T_r^{1/2})$)
			54+1.54226ω−0.26992ω
			4+

3. Modeling

This section describes the SFE calculation model used in this work. The generalized method is used by ThermoFAST [21] and other software programs capable of SFE calculations, such as MultiFlash [71]. The generalized three-parameter cubic EoS is formulated as follows:

$$p = \frac{RT}{v - b_m} - \frac{a_m}{v^2 + (b_m + c_m)v - b_m c_m} \qquad (1)$$

Here p is pressure, $R = 8.3144626\ \mathrm{J \cdot K^{-1} \cdot mol^{-1}}$ is the gas constant, T is temperature, and v is molar volume. For mixtures, the parameters a_m, b_m and c_m are calculated as averages over the component pure substances using the van der Waals mixing rules:

$$\begin{aligned} a_m &= \sum_i \sum_j x_i x_j a_{ij} \\ a_{ij} &= \left(1 - k_{ij}\right) \cdot \sqrt{a_i \cdot a_j} \\ b_m &= \sum_i x_i b_i \\ c_m &= \sum_i x_i c_i \end{aligned} \qquad (2)$$

where x_i is the mole fraction of component i. The binary interaction parameter k_{ij} is considered constant for each binary in this work. The pure component parameters a_i, b_i and c_i are calculated as follows:

$$\begin{aligned} a_i &= \alpha\left(T_{\mathrm{r},i}, \omega_i\right) \cdot \Omega_{\mathrm{a}} \frac{R^2 T_{\mathrm{C},i}^2}{p_{\mathrm{C},i}} \\ b_i &= \Omega_{\mathrm{b}} \frac{R T_{\mathrm{C},i}}{p_{\mathrm{C},i}} \\ c_i &= \Omega_{\mathrm{c}} \frac{R T_{\mathrm{C},i}}{p_{\mathrm{C},i}} \end{aligned} \qquad (3)$$

Here $T_{\mathrm{r},i} = T/T_{\mathrm{C},i}$ is the reduced temperature for component i, while $T_{\mathrm{C},i}$, $p_{\mathrm{C},i}$ and ω_i are the critical temperature, critical pressure, and acentric factor respectively. These values were obtained from

the software package REFPROP 10.0 [69] and are listed in Table 2. The function $\alpha(T_{r,i}, \omega_i)$ and the parameters Ω_a, Ω_b and Ω_c are EoS-specific; they are listed in Table 3. For a fluid mixture described by the generalized three-parameter cubic EoS, the fugacity coefficient of the component i in the fluid (liquid or vapor) phases φ_i^F is:

$$\ln\varphi_i^{\mathrm{F}} = -\ln\left(Z-B\right)+\frac{B_i}{Z-B}-\left[\frac{\sum_j x_j A_{ij}}{D}\ln\left(\frac{Q+D}{Q-D}\right)\right]+\left(\frac{A\left(B_i+C_i\right)}{2\left(Q^2-D^2\right)}\right)$$
$$+\left[\frac{A}{8D^3}\left\{C_i\left(3B+C\right)+B_i\left(3C+B\right)\right\}\right]\left\{\ln\left(\frac{Q+D}{Q-D}\right)-\frac{2QD}{Q^2-D^2}\right\} \quad (4)$$
$$\text{where: } Q=\left[Z+\frac{B+C}{2}\right], D=\sqrt{BC+\frac{\left(B+C\right)^2}{4}},$$
$$Z=\frac{vp}{RT}, A_i=\frac{a_i p}{R^2T^2}, A_{ij}=\frac{a_{ij}p}{R^2T^2}, B_i=\frac{b_i p}{RT}, C_i=\frac{c_i p}{RT}, A=\frac{a_m p}{R^2T^2}, B=\frac{b_m p}{RT}, C=\frac{c_m p}{RT}$$

Here Z is the compressibility factor. For pure components, the fugacity coefficient $\varphi_{\mathrm{pure}}^{\mathrm{F}}$ in the fluid (liquid or vapor) phase is:

$$\ln\varphi_{\mathrm{pure}}^{\mathrm{F}} = \left(Z-1\right)-\ln\left(Z-B\right)+\frac{A}{2U}\ln\left(\frac{Z+M}{Z+V}\right)$$
$$\text{where: } U=-\sqrt{BC+\frac{(B+C)^2}{4}},\ M=\frac{(B+C)}{2}-U,\ V=\frac{(B+C)}{2}+U \quad (5)$$

The solid phase is assumed to be a pure substance, and the fugacity coefficient of this pure component is calculated with [72]:

$$\ln\varphi_{\mathrm{pure}}^{\mathrm{S}} = \ln\left(\phi_{\mathrm{pure}}^{\mathrm{L}}\right)-\frac{\Delta H_{\mathrm{f}}}{RT_{\mathrm{m}}}\left[\frac{T_{\mathrm{m}}}{T}-1\right]+\frac{\Delta c_{\mathrm{p}}}{R}\left[\frac{T_{\mathrm{m},i}}{T}-1+\ln\left(\frac{T}{T_{\mathrm{m}}}\right)\right]-\frac{\Delta v\left(p-p_{\mathrm{m}}\right)}{RT} \quad (6)$$

Here $\varphi_{\mathrm{pure}}^{\mathrm{L}}$ is the fugacity coefficient of the pure component in the liquid phase, and p_{m} is the reference pressure (triple point pressure for carbon dioxide and atmospheric pressure for the remaining components). For a pure component at p_{m}, T_{m} is the melting temperature, ΔH_{f} is the

heat of fusion, Δc_p ($= c_p^L - c_p^S$) is the change of the isobaric heat capacity from solid to liquid phase and Δv is the change in molar volume from solid to liquid phase. The values of these parameters for each pure component were estimated from the DIPPR® 801 database [70] and are listed in Table 2. It is important to note that the pure fluid properties Δc_p and Δv are generally experimentally determined at a single temperature and pressure, most commonly the normal melting point. Theoretically, these values should be an average over the temperature and pressure range from the mixture SFE condition to the pure substance triple point. The errors in this assumption are compensated for by the fitting of the binary interaction parameters used to calculate the fugacity of the solute in the fluid phase. The result of the error compensation in the binary mixture description can be larger errors when the fitted k_{ij} values are used to predict phase behavior in multicomponent mixtures. This illustrates the need for high-quality experimental data for pure substances as well as for binary mixtures.

As described by Parks et al. [73], cyclohexane experiences a solid-solid crystalline transition at T_{tran} = 185.9 K and atmospheric pressure. For mixtures containing cyclohexane at temperatures higher than T_{tran}, the fugacity coefficient of pure cyclohexane can be calculated with Eq. (6); while at temperatures lower than T_{tran}, the following modification should be used [9]:

$$\ln \varphi_{pure}^{S} = \ln\left(\phi_{pure}^{L}\right) - \frac{\Delta H_f}{RT_m}\left[\frac{T_m}{T} - 1\right] + \frac{\Delta c_p}{R}\left[\frac{T_{m,i}}{T} - 1 + \ln\left(\frac{T}{T_m}\right)\right] - \frac{\Delta v\left(p - p_m\right)}{RT} - \frac{\Delta H_{S,tran}}{RT_{tran}}\left[\frac{T_{tran}}{T} - 1\right] \quad (7)$$

where $\Delta H_{S,tran}$ = 6715 J·mol^{-1} is the enthalpy of the cyclohexane crystalline phase transition at T_{tran}.

At SFE, the fugacity of component *i* is equal in all phases, i.e. for a single fluid phase at equilibrium with a solid, the following relation holds

$$\varphi_{\text{pure}}^{\text{S}} = x_i^{\text{F}} \cdot \phi_{\text{pure},i}^{\text{F}} \tag{8}$$

Here, x_i^{F} is the mole fraction of component *i* in the fluid phase. The solubility of an impurity in a binary mixture with methane can be calculated from a specified temperature and pressure by solving the system of equations comprised of Eqs. (1) to (8) and $x_1 + x_2 = 1$. Similarly the SFE temperature of a binary methane mixture can be calculated from a specified composition and pressure.

When three-phases are present at equilibrium (e.g. SLVE), the following equations hold

$$\varphi_{\text{pure}}^{\text{S}} = x_i^{\text{L}} \cdot \phi_{\text{pure},i}^{\text{L}} = x_i^{\text{V}} \cdot \phi_{\text{pure},i}^{\text{V}} \tag{9}$$

Here, x_i^{L} and x_i^{V} are the mole fractions of component *i* in the liquid phase and vapor phase, respectively. Instead of analytically solving the system of equations describing SLVE, a bisection method incorporating a robust flash algorithm (which determines two-phase equilibrium condition of a mixture at the given overall composition, pressure and temperature) proposed by Baker et al. [7, 9] was adopted. The bisection method requires flash calculations in the order of 10 times which make it slower than calculating SLE and SVE conditions.

As mentioned in the introduction, the EoS models considered in this paper have been implemented within the *ThermoFAST* program. In addition to the desktop version [21], which was first released in 2018, a web application version, *ThermoFAST Web* [23] containing the tuned models detailed in this work, has recently been developed and is available online via the link: https://thermofastweb.azurewebsites.net. Figure 2 illustrates a screenshot of *ThermoFAST Web* [23], showing model selection.

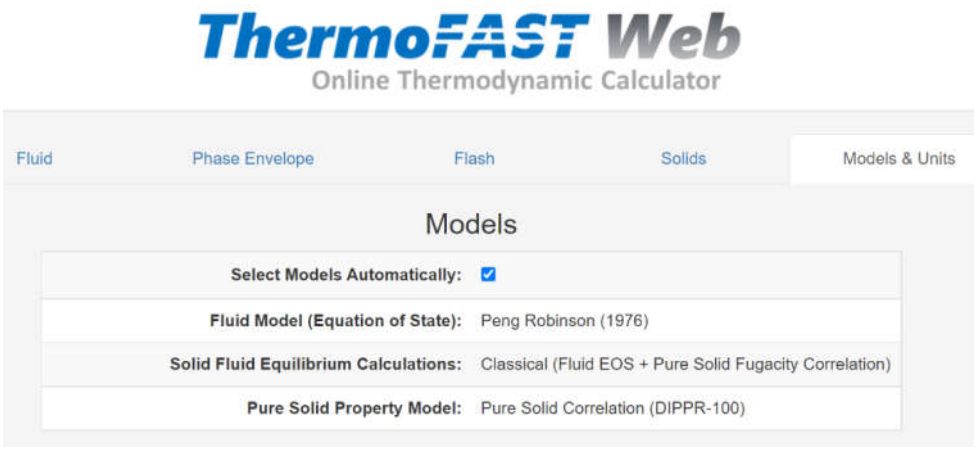

Figure 2. Illustrative screenshot of *ThermoFAST Web* [23], showing model selection.

4. Results

4.1 Pure Component Calculations

The reliability of each selected EoS for phase equilibrium calculations was first investigated using pure components. The performance of each EoS was evaluated by comparing the predicted triple point temperature T_{tr} at the intersection point of the calculated SLE and solid-vapor-equilibrium (SVE) curves to the reference triple point temperature obtained from REFPROP 10.0 [69]. The deviations for all pure components are presented in Figure 3. The predicted T_{tr} with the PR, SRK, PTV and PRSV EoS are almost the same for all pure components and have similar deviations from the reference values. The WRK and RK EoS only work well for some pure components; for some others, e.g., toluene, the deviations exceed the limit of Figure 3. This is attributable to the poor convergence of SVE calculations at conditions near the triple point when the WRK or RK EoS are used.

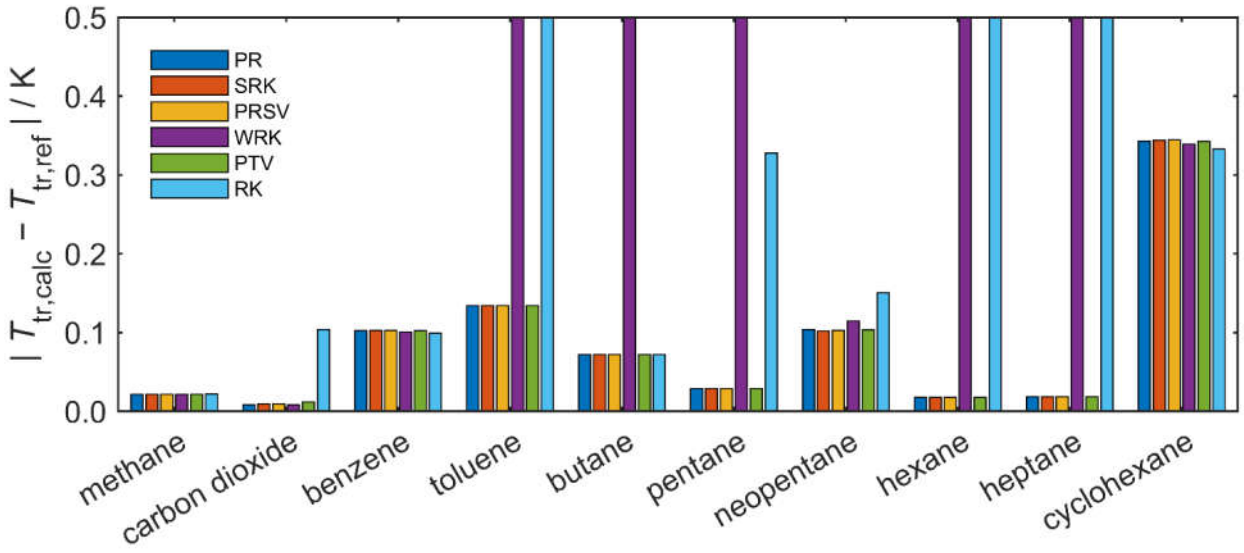

Figure 3. Difference between the calculated triple point temperature ($T_{tr,calc}$) and the reference triple point temperature ($T_{tr,ref}$) as obtained from REFPROP 10.0 [69].

4.2 Determination of best-fit binary interaction parameters

For the SFE calculation described in Section 3, the binary interaction parameter, k_{ij}, is the most important adjustable parameter. A first approximation for the value of k_{ij} to use in SFE calculations is the $k_{ij,VLE}$ that optimises VLE calculations for that binary system. The value of k_{ij} which optimises the model's ability to represent experimental VLE data for a given binary is not, however, necessarily the same as the value that optimises the model's ability to represent experimental SFE data. This is because in both cases the model is making an approximate estimate of the component's fugacity in each equilibrium phase and then determining the condition at which those two approximate estimates are equivalent. In the case of a VLE calculation, the same equation (Eq. (4)) is used to estimate the fugacities of the component at two different fluid densities, while in the case of an SFE calculation two different equations (namely Eq. (6) for the solid and Eq. (4) for the fluid) are used to generate the estimates. In all cases, the values of the fugacities calculated are not necessarily accurate; they just need to be equal at the phase equilibrium condition observed experimentally. Thus, the value of k_{ij} determined by regression of

the model to the available experimental SFE data corresponds to that which forces the cubic EOS for the binary mixture to match the fugacity estimated for the solid phase using Eq. (6). The value of k_{ij} determined in this work (and in others) as merely as a fitting parameter that forces agreement between the particular model and the limited experimental SFE data available. We found that it was sufficient to treat the k_{ij} as a constant, with no temperature and composition dependence [74, 75].

To determine the best-fit k_{ij} for each EoS and binary system, the objective function chosen was the root-mean-square RMS_T deviation:

$$\mathrm{RMS}_T\left(k_{ij}\right)=\sqrt{\frac{\sum_{l=1}^{N}\left[T_{\mathrm{exp},l}-T_{\mathrm{calc},l}\left(k_{ij}\right)\right]^2}{N}} \tag{10}$$

where T_{exp} is the experimental SFE temperature, T_{calc} is calculated with the cubic EoS, and l is an index over the N experimental data points. The value of k_{ij} was varied over a large range (typically from −0.2 to 0.2) with an interval step size of 0.001, with the best-fit k_{ij} value being that which yielded the minimum $\mathrm{RMS}_{T,\mathrm{min}}$. An initial best-fit k_{ij} was determined using all experimental values in the fitting. This initial k_{ij} was then used to identify and remove experimental values deviating from the calculation by more than 8.0 K (more than two times of the expanded uncertainties of all EoS for all binary systems, as discussed in Section 4.3). The remaining experimental values were used in a second round of fitting. The values of RMS_T in the second round of fitting are plotted as a function of k_{ij} in Figure 4. The shape curves indicates that the RMS_T is very sensitive to k_{ij} (*i.e.*, increasing or decreasing k_{ij} results in a significant increase of RMS_T) for the methane binary mixtures with benzene, toluene, pentane, hexane, heptane and cyclohexane for all EoS. The main reason for this high sensitivity is that at a given composition and pressure both SLE and SVE conditions can exist but with disparate equilibrium temperatures. A small change in k_{ij} can then

cause the calculation to converge the wrong equilibrium condition which occurs at a significantly different temperature to the measured condition, thereby increasing the RMS_T considerably. For methane binary mixtures with carbon dioxide, butane, and neopentane, the RMS_T is sensitive to increases in k_{ij} from its optimized value, but is insensitive to decreases.

The best-fit k_{ij} and corresponding $RMS_{T,min}$ for each EoS and binary system are tabulated in Table 4, and $RMS_{T,min}$ is illustrated in Figure 5. All EoS predict the SFE with $RMS_{T,min}$ on the order of 2.0 K for the binary methane mixtures with butane and pentane. In general, the PR, SRK, PTV and PRSV EoS with their individual best-fit k_{ij} yield the lowest $RMS_{T,min}$ (on the order of 2.0 K) among the six EoS for all binary methane mixtures except for that with toluene and cyclohexane. The WRK EoS has the lowest $RMS_{T,min}$ for the binary methane mixture with toluene and cyclohexane but yields very high values for mixtures with benzene and neopentane. The predictions of the RK EoS are poor for most of the mixtures. In summary, the PR, SRK, PTV and PRSV EoS are satisfactory for all the investigated binary mixtures, while the WRK EoS is the best choice for the binary mixture of methane with toluene and cyclohexane.

The comparison between the k_{ij} of the PR EOS optimized for the SLE data to those optimized for the VLE data, $k_{ij,VLE}$, [21] is illustrated in Figure 6. In general, the two values are similar for most of the methane binary mixtures except for those with butane and neopentane. Given the discussion above, this agreement is encouraging because it indicates a level of consistency between the estimates of solid phase fugacity with Eq. (6) and the estimates of that component's fugacity in a fluid phase. For the two discrepant compounds it suggests that there might be an issue with one or more of the pure substance parameters on the right-side of Eq. (6), and/or that additional experimental SFE data need to be acquired for these binary mixtures.

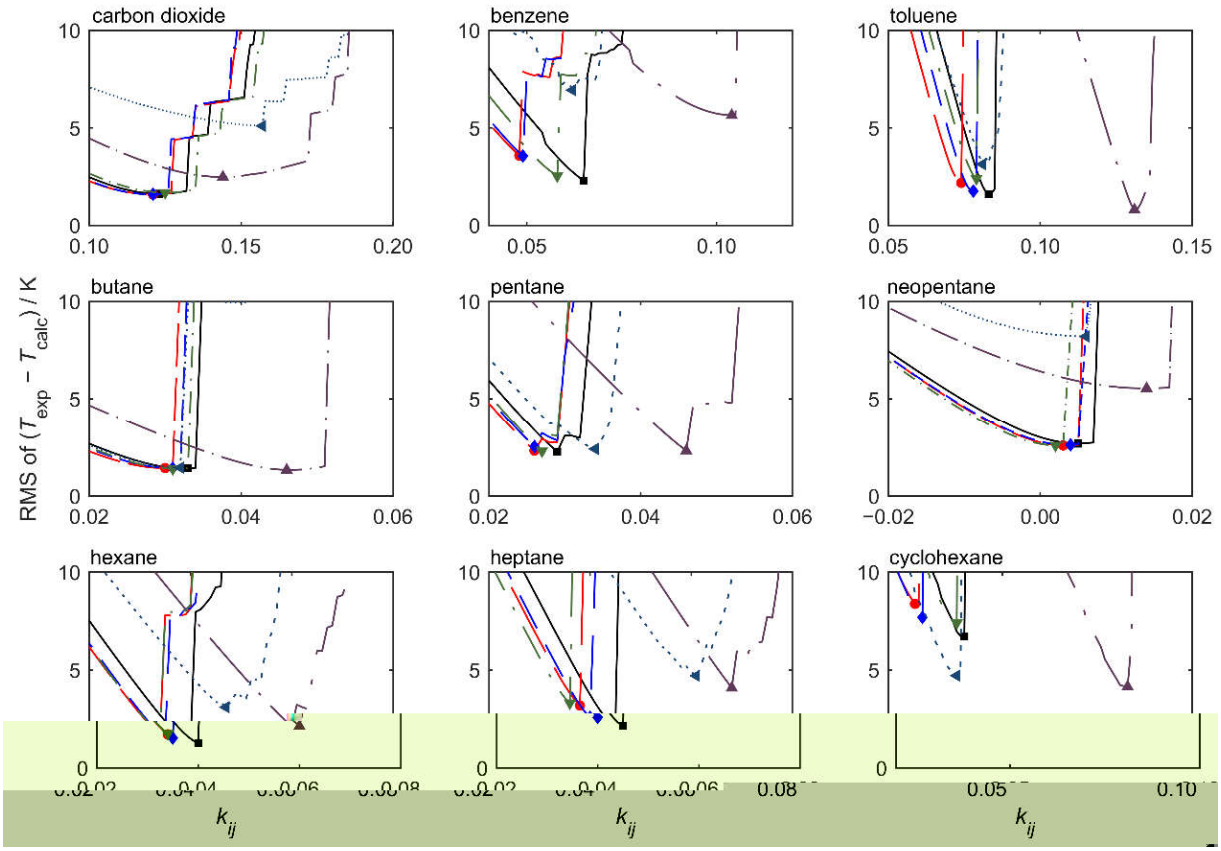

Figure 4. The root-mean-square (RMS) of the difference of the experimental solid-fluid-equilibria temperature T_{exp} of the methane binary mixtures from values T_{calc} calculated with the cubic EoS at different binary interaction parameters k_{ij}. PR: solid curve and ■; SRK: long dashed curve and ● ; PRSV: short dashed curve and ◆; WRK: long dashed dotted curve and ▲; PTV: short dashed dotted curve and ◂; RK: dotted curve and ▼. The symbol denotes the minimum value on each curve.

Table 4. The best-fit binary interaction parameter k_{ij} for methane binary mixtures, and root-mean-square RMS_T of the difference between the experimental and the calculated solid-fluid equilibrium temperatures.

Solute		PR	SRK	PRSV	WRK	PTV	RK
carbon dioxide	k_{ij}	0.123	0.121	0.121	0.144	0.125	0.157
	RMS_T / K	1.623	1.589	1.594	2.485	1.683	5.103
benzene	k_{ij}	0.065	0.048	0.049	0.104	0.058	0.062
	RMS_T / K	2.290	3.583	3.556	5.650	2.536	6.938
toluene	k_{ij}	0.083	0.074	0.078	0.131	0.079	0.081
	RMS_T / K	1.605	2.181	1.758	0.809	2.404	3.139
n-butane	k_{ij}	0.033	0.030	0.031	0.046	0.031	0.032
	RMS_T / K	1.411	1.425	1.423	1.330	1.387	1.444
n-pentane	k_{ij}	0.029	0.026	0.026	0.046	0.027	0.034
	RMS_T / K	2.253	2.315	2.532	2.312	2.295	2.402
neopentane	k_{ij}	0.005	0.003	0.004	0.014	0.002	0.006
	RMS_T / K	2.679	2.582	2.612	5.549	2.580	8.210
n-hexane	k_{ij}	0.040	0.034	0.035	0.060	0.034	0.047
	RMS_T / K	1.288	1.723	1.529	2.137	1.757	3.106
n-heptane	k_{ij}	0.045	0.038	0.040	0.068	0.036	0.061
	RMS_T / K	2.160	3.190	2.587	4.091	3.319	4.709
cyclohexane	k_{ij}	0.040	0.027	0.029	0.083	0.038	0.038
	RMS_T / K	6.726	8.381	7.691	4.152	7.401	4.717

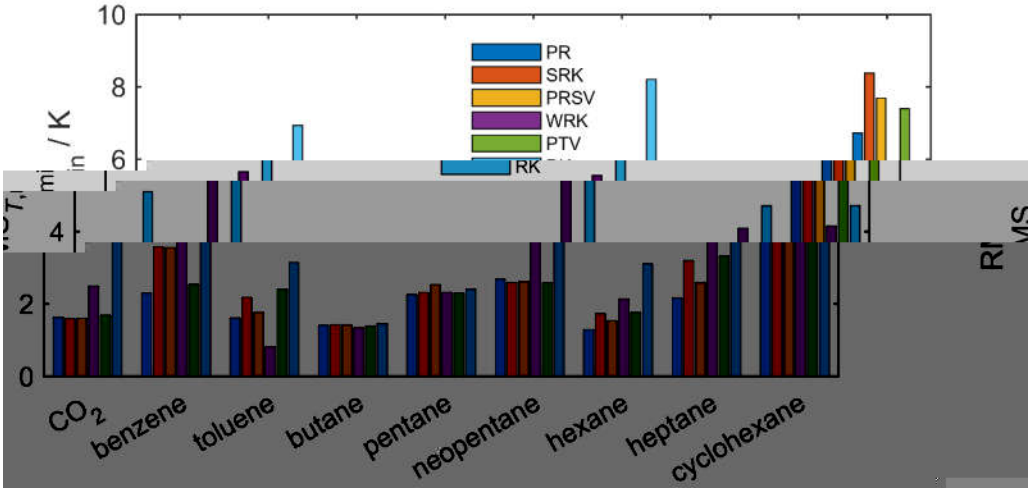

Figure 5. The root-mean-square $RMS_{T,min}$ of the difference between experimental solid-fluid equilibrium temperatures and the values calculated with the cubic EoS using the best-fit binary interaction parameters k_{ij} for the methane binary mixtures.

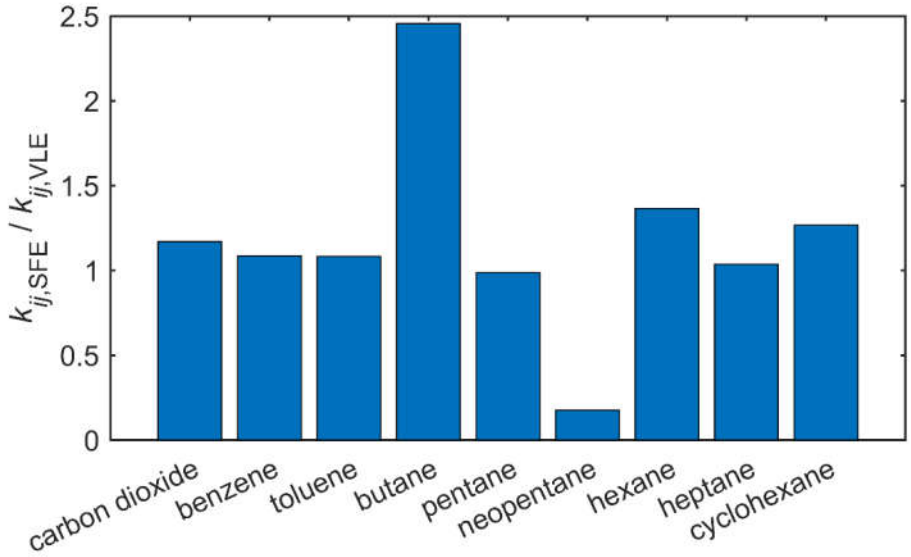

Figure 6. The ratio of the best-fit binary interaction parameters for the PR EOS fitted to the SFE data, $k_{ij,SFE}$, for methane binary mixtures in this work to those, $k_{ij,VLE}$, fitted to the VLE data obtained from ThermoFast [21].

4.3 Evaluation of experimental data

One metric to assess the overall quality of the experimental data is the ratio of the number of values used in the second round of fitting to the total number of values available (see Table 1 and Figure 1). Since the first round of fitting served to remove values that deviated largely from the set, a higher ratio indicates better quality. As shown in Figure 1, for binary methane mixtures with carbon dioxide, pentane, hexane and cyclohexane more than 90 % of the experimental data were used in the second round of fitting. This implies that the experimental data for these three systems are generally consistent with each other. Less than 80 % of the experimental data were used for binary methane mixtures with neopentane and heptane, mainly due to the high scatter of certain data sources. For binary methane mixtures with butane, toluene, and benzene, 80 % to 90 % of the experimental data were used; however, the butane and toluene datasets are limited to fewer than 50 values each.

The deviations of the experimental SFE temperatures, T_{exp}, from the calculated values, T_{calc}, using the PR EoS are presented in Figure 7. The PR EoS was chosen because it is one of the most accurate of the EoS investigated. The expanded uncertainty ($k = 2$) of the PR EoS in SFE temperature calculation for each binary system is estimated as:

$$U(T) = 2 \cdot \sqrt{\frac{1}{N}\sum_{l=1}^{N}\left[\left(T_{\mathrm{exp},l} - T_{\mathrm{calc},l}\right) - \alpha\right]^2}$$
$$\alpha = \frac{1}{N}\sum_{l=1}^{N}\left(T_{\mathrm{exp},l} - T_{\mathrm{calc},l}\right) \qquad (11)$$

The result is less than 4.0 K for all the investigated binary methane mixtures except the one with neopentane (5.0 K) and with cyclohexane (10.0 K). Similar uncertainties were obtained for the SRK, PTV and PRSV EoS, but significantly higher uncertainties were calculated for the other two EoS.

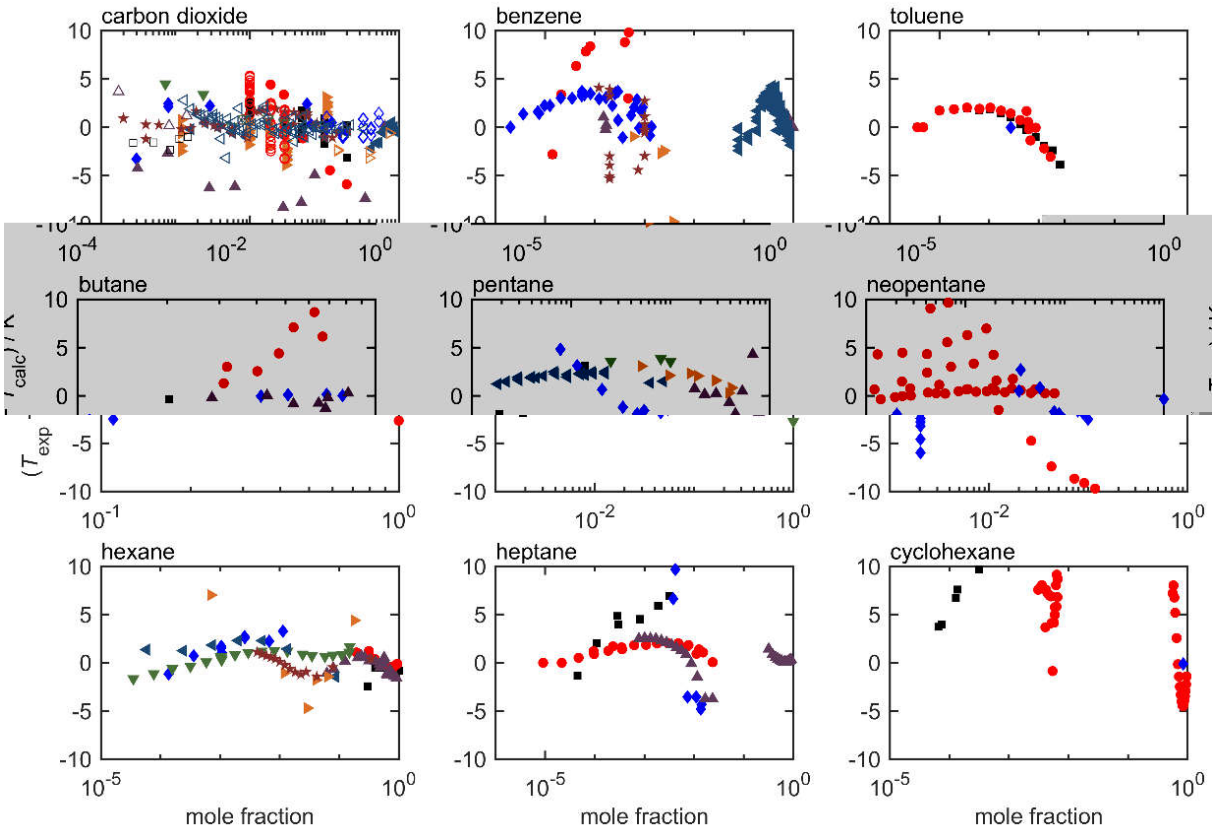

Figure 7. Absolute deviations of the experimental solid-fluid equilibria temperature T_{exp} of methane binary mixtures from values T_{calc} calculated with the PR EoS. **Carbon dioxide:** ■Pikaar [29], ●Sterner [30], ◆Cheung & Zander [31], ▲Streich [32], ▼Preston *et al.* [33], ◂Kurata [34], ▸Agrawal & Laverman [35], ★Voss [36], □Sparks & Sloan [37], ○Boyle [38], ◇Le & Trebble [39], △Zhang *et al.* [40], ▽Gao *et al.* [41], ◁Shen *et al.* [42], ▷Xiong *et al.* [43], ☆Stringari *et al.* [44]. **Benzene:** ■Neumann & Mann [45], ●Neumann *et al.* [46], ◆Kuebler & McKinley [47], ▲Luks *et al.* [48], ▼Teller & Knapp [49], ◂Rijkers *et al.* [50], ▸Hughes *et al.* [51], ★ Siahvashi *et al.* [52]. **Toluene:** ■ Kuebler & McKinley [47], ●Kurata [53], ◆Luks *et al.* [54]. **Butane:** ■Morlet [55], ●Kurata [53], ◆Kuebler & McKinley [56], ▲Brew [57]. **Pentane:** ■Morlet [55], ●Preston *et al.* [33], ◆Boyle [58], ▲Dickinson [59], ▼Kurata [53], ◂Kuebler & McKinley [56], ▸Brew [57]. **Neopentane:** ■Preston *et al.* [33], ●Baughman *et al.* [60], ◆Siahvashi *et al.* [61]. **Hexane:** ■Beck [62], ●Shim & Kohn [63], ◆ Neumann & Mann [45], ▲Dickinson [59], ▼Kuebler & McKinley [47], ◂de Mateo & Kurata [64], ▸Brew [57], ★Luks *et al.* [48]. **Heptane:** ■Neumann & Mann [45], ● Kuebler & McKinley [47], ◆Kohn & Luks [65], ▲ Tiffin *et al.* [66]. **Cyclohexane**: ■Neumann & Mann [45], ● Kohn *et al.* [67], ◆Jasperson *et al.* [68].

4.4 Phase envelope predictions and *retrograde* solidification

In this section, phase diagrams in the *p-T* plane of selected binary mixtures involving solid, liquid, vapor phases and the supercritical region were investigated to identify which types of data (SLE, SVE or SLVE) should be acquired to better constrain models, to show the differences of the six EoS in calculating the phase diagrams, and to study the various retrograde behaviors of the solid phase.

Phase diagrams showing all three phases are shown for three binary mixtures (0.9004 methane + 0.0996 neopentane), (0.90 methane + 0.10 carbon dioxide), and (0.9999 methane + 0.0001 benzene) in Figure 8, Figure 9, and Figure 10, respectively. These mixtures were chosen as there are experimental data from multiple sources measured at similar compositions on at least two of the SLVE, SLE, and SVE conditions. The SVE and SLE curves calculated with all six EoS using their best-fit k_{ij} are shown; however to avoid over-complicating the figure the LVE and SLVE curves were calculated with the PR EoS only. It should be noted that calculations near critical points might not be reliable; this is a known shortcoming of cubic EoS.

To generate these phase diagrams, the SLVE curve of each binary system was first calculated. The SLVE condition for a binary mixture has only one degree of freedom, so once a temperature is specified the convergence of the flash calculation to the corresponding pressure, if an SLVE condition exists, is insensitive to the specified composition of the binary system. For a binary system of fixed composition, the high temperature bound of the SLVE curve occurs at the intersection of the dew (VLE) and frost (SVE) curves (see Figure 8 and Figure 9). The cubic EoS is able to calculate the extensions of the SVE and VLE curves through this high temperature bound; however these extensions are not physical. The SLVE curve also passes through the intersection of the bubble (VLE) and melting (SLE) curves at low temperatures. At temperatures below this

intersection, the SLVE curve continues to lower pressures, dividing the SLE and SVE regions. These three phase diagrams provide insight into the relative information content of measurements acquired to optimize binary interaction parameters for the SFE calculations. Experimental data on the SVE curve are generally more valuable than those on the SLE curve, as a SLE curve is generally insensitive to pressure. Experimental data on the SLVE curve of a binary system do not contain composition information and thus do not require its measurement. Temperature and pressure data measured on the SLVE curve of a binary system can provide useful constraints on predictive models. However, measurements on a binary mixture's SLVE curve at temperatures below the intersection of the SLE and LVE curves have low information content unless the overall composition and the amount of solid present are well-known.

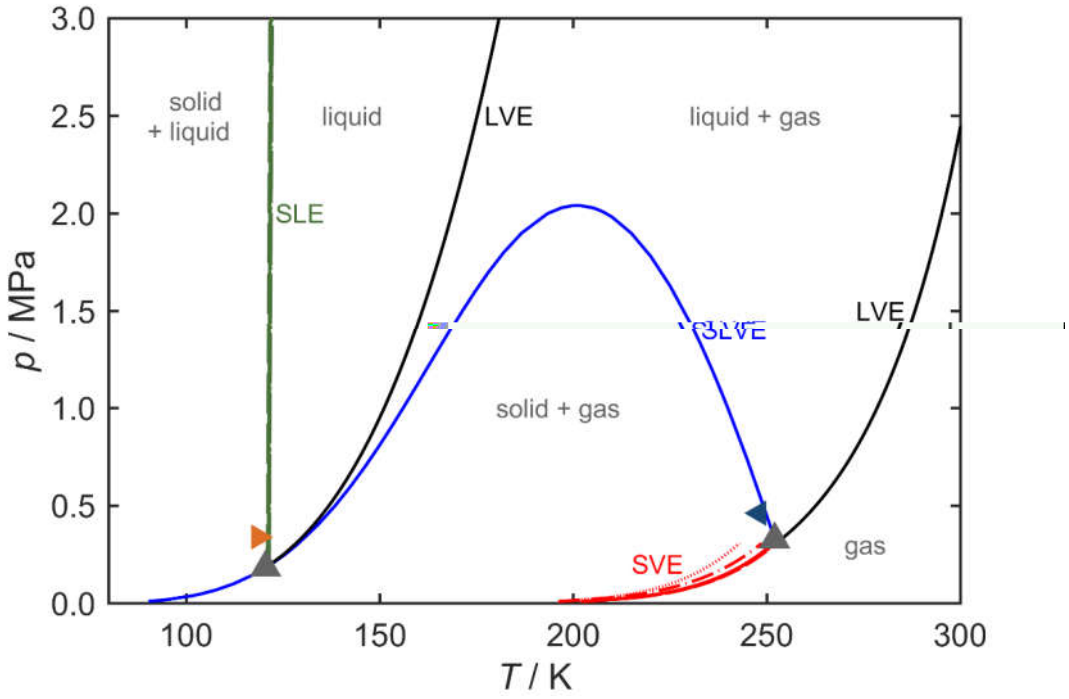

Figure 8. The *p*-*T* phase diagram of the binary (0.9004 methane + 0.0996 neopentane) mixture. All solid curves were calculated with the PR EoS; SVE and SLE curves were calculated with all six EoS (PR: solid curve; SRK: long dashed curve; PRSV: short dashed curve; WRK: long dashed dotted curve; PTV: short dashed dotted curve; RK: dotted curve) with their best-fitted binary interaction parameters. Symbols: ▸ experimental data of Siahvashi *et al.* [61]; ◂ experimental data

of Baughman *et al.* [60] for this binary mixture with neopentane mole fraction 0.0909. ▲, intersection points.

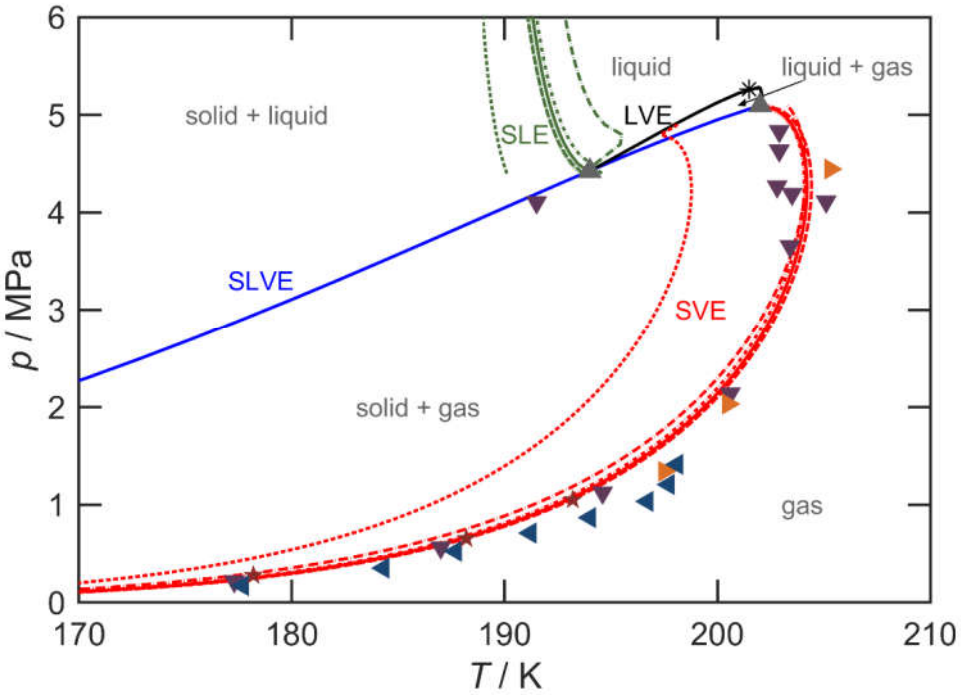

Figure 9. The *p*-*T* phase diagram of the binary (0.90 methane + 0.10 carbon dioxide) mixture. All solid curves were calculated with the PR EoS; SVE and SLE curves were calculated with all six EoS (PR: solid curve; SRK: long dashed curve; PRSV: short dashed curve; WRK: long dashed dotted curve; PTV: short dashed dotted curve; RK: dotted curve) with their best-fitted binary interaction parameters. Symbols: experimental data of ▼Pikaar [29], ◂Agrawal & Laverman [35], ▸Zhang *et al.* [40] and ★Xiong *et al.* [43] with carbon dioxide mole fraction from 0.09 to 0.11. ▲, intersection points; *, critical point.

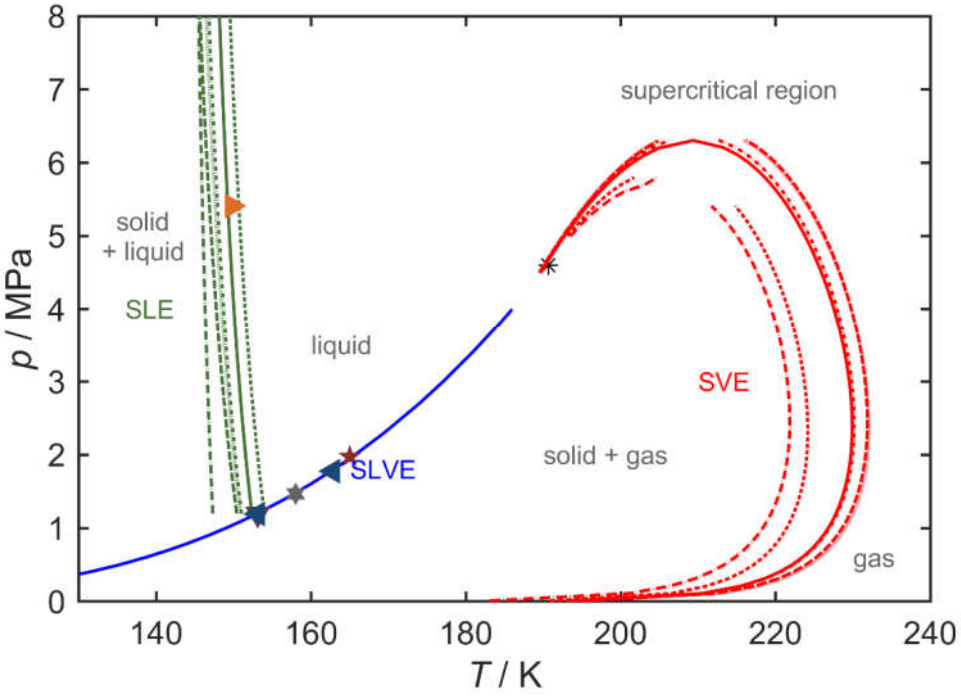

Figure 10. The *p*-*T* phase diagram of the binary (0.9999 methane + 0.0001 benzene) mixture. All solid curves were calculated with the PR EoS; SVE and SLE curves were calculated with all six EoS (PR: solid curve; SRK: long dashed curve; PRSV: short dashed curve; WRK: long dashed dotted curve; PTV: short dashed dotted curve; RK: dotted curve) with their best-fitted binary interaction parameters. Symbols: experimental data of ▼Neumann & Mann [45], ◂Neumann *et al.* [46], ▸Kuebler & McKinley [47] ★ Luks *et al.* [48] ✶Teller & Knapp [49] with benzene mole fraction from 0.00008 to 0.00012; *, critical point.

Experimental data for mixtures with similar compositions are also shown in Figure 8 to 10. No experimental pressures are reported for SLVE data acquired for the (0.9999 methane + 0.0001 benzene) system. When the predicted (extrapolated) bubble point curve is effectively coincident the SLVE curve, data measured under the latter conditions again have relatively low information content. For the (0.9004 methane + 0.0996 neopentane) and (0.90 methane + 0.10 carbon dioxide) mixtures, the PR, SRK, PTV and PRSV EoS yield similar predictions of the SVE and SLE curves and generally agree well with the experimental data. In contrast, the curves predicted with the WRK and RK EoS exhibit obvious deviations. For the (0.9999 methane + 0.0001 benzene)

mixture, the scatter in the SLE curves calculated with all six EoS is about 7 K, while the scatter in the calculated SVE curves is even larger (11 K). Among all EoS, the PR and PRSV EoS produce the best agreement with the single available SLE data point.

Retrograde solidification behavior can be observed for all three investigated mixtures, albeit in very different scenarios. If the (0.9004 methane + 0.0996 neopentane) mixture shown in Figure 8 is cooled at a constant pressure of 1.0 MPa, the solid phase will first appear in the gas-liquid mixture. This is normal solidification with the amount of solid increasing as temperature decreases; however, in this case a further reduction in temperature will cause the amount of liquid phase present to decrease. Hence this transition corresponds toi%

dissolve back into a supercritical dense phase (SVE to liquid, pathway #15) and eventually re-appear from the liquid (liquid to SLE, pathway #5). Figure 13 of Baker et al. [9] presents additional examples of the multiple types of solid-fluid transition pathways that can occur in the methane + benzene binary at different compositions.

4.5 Solubility Calculations

Determination of best-fit binary interaction parameters, as described in Section 4.2, allows accurate prediction of SFE temperature at fixed pressure and composition. In this section, solubility calculations at given pressure and temperature are examined using the exemplar PR EoS with the corresponding optimized k_{ij}. Experimental solubility is defined here as the fluid-phase mole fraction of the impurity in the binary methane mixture at SFE conditions. Figure 11 shows experimental data, measured over a wide range of pressures, for the solubility of multiple impurities in methane as a function of temperature. The curves shown in Figure 11 are the SLE predictions for each binary system, calculated at a constant pressure of p = 11 MPa. The experimental data generally agree well with the calculated constant pressure SLE curves, primarily because SLE conditions are generally insensitive to pressure. There are two component sets of reliable experimental data which demonstrate a large deviation from the calculated isobaric SLE curves. The first (Figure 11a) are for the methane + benzene binary measured at high temperature (> 250 K) and very high pressure (approximately 40 MPa) SFE conditions [50]. At these super-critical conditions, the data indicate that the solubility of benzene in methane is significantly larger than at 11 MPa. (The model correctly predicts these SFE data if the experimental pressures are used as inputs rather than 11 MPa).

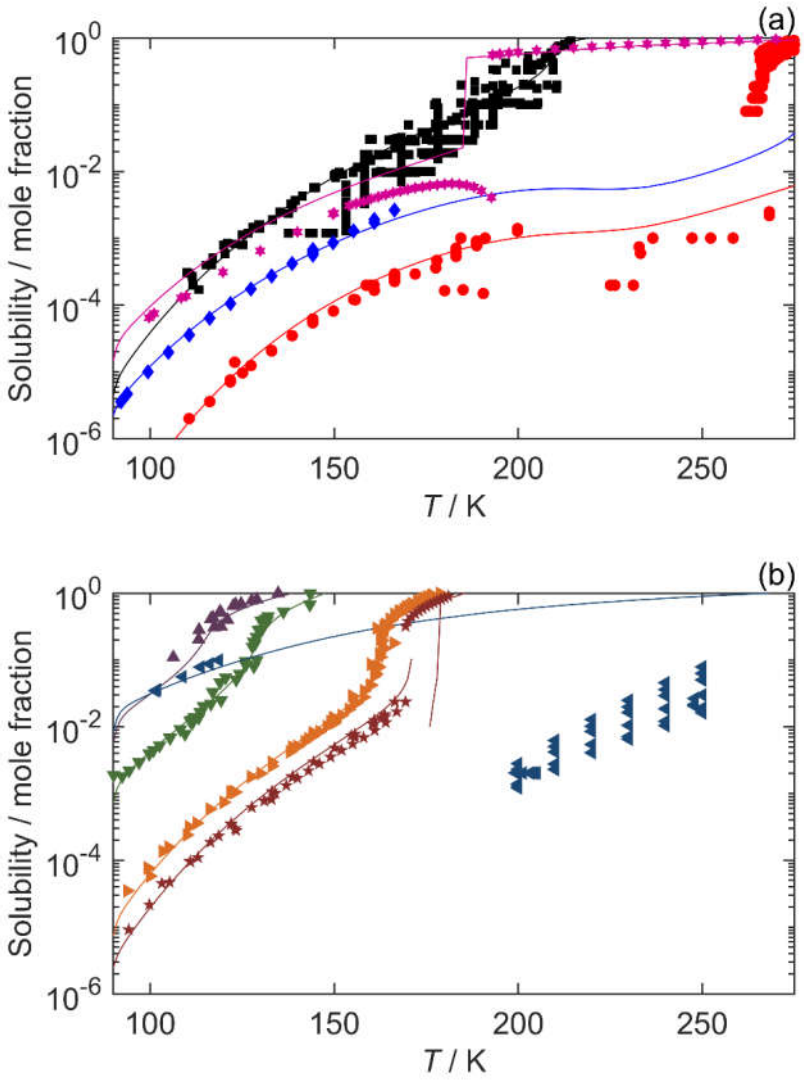

Figure 11. Solubility of each impurity in methane. The symbols (■ carbon dioxide, ● benzene, ◆ toluene, ▲ butane, ▼ pentane, ◂ neopentane, ▸ hexane, ★ heptane, ✶ cyclohexane) are experimental data from literature. The curves are isobaric SLE curves calculated with the PR EoS using the best-fit binary interaction parameters at a pressure of 11 MPa.

The second data set exhibiting a significant deviation from the isobaric SLE solubility curve occurs for the methane + neopentane binary (Figure 11b). The SVE and SLVE data measured by Baughman et al. [60] in the pressure range (0.3 to 3.1) MPa have neopentane solubilities approximately two orders of magnitude smaller than those calculated at 11 MPa (no data at 11

MPa are available in this temperature range to confirm the model's SFE predictions). This implies that the risk of neopentane solidification in natural gas mixtures is largest at higher temperatures, where SVE conditions occur, rather than conditions where the natural gas has been (partially) liquefied.

As shown in Figure 11, solubility of the impurities generally decreases with decreased temperature. At temperature T = 123 K (typical effluent condition of the main cryogenic heat exchanger in an LNG plant [10]), the solubility in mole fraction of each component reduces from 0.1 to 0.00001 in the sequence: *n*-butane, neopentane, *n*-pentane, *n*-hexane, carbon dioxide, *n*-heptane, toluene, and benzene. Benzene has the highest risk of solidification over almost the entire temperature range relevant to LNG production. The solubility of benzene is predicted to be < 1 ppm at temperatures lower than approximately 110 K.

5. Conclusions

The solid-fluid-equilibrium (SFE) of mixtures relevant to liquefied natural gas (LNG) applications has been investigated via the analysis of binary mixtures of methane with carbon dioxide, benzene, toluene, *n*-butane, *n*-pentane, neopentane, *n*-hexane, *n*-heptane or cyclohexane. A summary of the available experimental SFE data has been provided, and binary interaction parameters of six cubic equations of state (EoS) have been determined for each system. The Peng-Robinson (PR), Soave-Redlich-Kwong (SRK), PR-Stryjek-Vera (PRSV) and Patel-Teja-Valderrama (PTV) EoS are all able to represent the SFE data adequately, and were implemented into ThermoFAST and ThermoFAST Web applications. These EoS estimate the experimental SFE temperatures with standard uncertainties (k = 1) of less than 2 K for a specified pressure and compositions.

Additional experimental data for these and other binary mixtures relevant to LNG production are needed. To be of most utility to the development of reliable engineering models, experimental SFE

data report with temperature, pressure, equilibrium composition and equilibrium phases present. Data measured at SLVE conditions at temperatures above the SLE line can be very useful for constraining model predictions.

The review of the SFE data, which can be freely accessed through an online database [24], and their comparison with model predictions of solid-fluid phase behavior and solubility, reveal new insights regarding operational freeze-out risk, possible remediation strategies for blockages in cryogenic heat exchanger, as well as opportunities for future research. Neopentane is very soluble in liquid LNG but can be a significant freeze-out risk at higher temperatures where the methane is gaseous. The potential for retrograde solidification means that in some cases it may be possible to remediate benzene solids that have formed in cryogenic heat exchangers by reducing the bundle temperature. Finally, as hydrogen liquefaction becomes increasingly important to the global energy transition, similar issues regarding the ability to assess impurity freeze-out risk will need to be addressed through thermodynamic modelling and measurements.

Acknowledgements

The authors are grateful the Australian Research Council through the Industrial Transformation Training Centre for LNG Futures, IC150100019. Additionally, the authors would like to recognize the Gas Processors Association (GPA Midstream) for endorsement of the ThermoFAST software package and support of the compilation of the JESS Hydrocarbon Solubility Database. C.C.S. would like to acknowledge the financial support of the Australian Government and the American Australian Association.

References

[1] Global Natural Gas Markets Overview. Washington, D.C.: U. S. Energy Information Administration, prepared by Leidos, Inc.; August 2014. p. 7.
[2] Eggeman T, Chafin S. Beware the pitfalls of CO 2 freezing prediction. Chem Eng Prog. 2005;101:39-44.
[3] Ismail SM, Al-Thani K. Unique Phenomenon of Moisture & Other Contaminants' Coalescence under Cryogenic Conditions. Proceedings of LNG-18 Perth, Australia2016.
[4] GIIGNL Annual Report. Neuilly-sur-Seine, France: International Group of Liquefied Natural Gas Importers; 2019.
[5] Thurtell D, Pitts N, Harvey E, Gibbons M, Drahos N, Philalay M, et al. Resources and Energy Quarterly March 2020. In: Department of Industry S, Energy and Resources, editor.2020.
[6] Li H, Yan J. Evaluating cubic equations of state for calculation of vapor–liquid equilibrium of CO2 and CO2-mixtures for CO2 capture and storage processes. Applied Energy. 2009;86:826-36.
[7] Baker CJ, Oakley JH, Rowland D, Hughes TJ, Aman ZM, May EF. Rapid simulation of solid deposition in cryogenic heat exchangers to improve risk management in liquefied natural gas production. Energy & Fuels. 2018;32:255-67.
[8] Smith T, Doong S. Selective C5+ removal for lean feed gas. LNG Industry. 2016:15-8.
[9] Baker C, Siahvashi A, Oakley J, Hughes T, Rowland D, Huang S, et al. Advanced predictions of solidification in cryogenic natural gas and LNG processing. J Chem Thermodyn. 2019;137:22-33.
[10] Baker CJ, Oakley JH, Rowland D, Hughes TJ, Aman ZM, May EF. Rapid Simulation of Solid Deposition in Cryogenic Heat Exchangers To Improve Risk Management in Liquefied Natural Gas Production. Energy Fuels. 2018;32:255-67.
[11] Sloan ED, Koh CA. Clathrate Hydrates of Natural Gases. 3 ed. Boca Raton, Florida, USA: CRC Press; 2007.
[12] Makogon IF, Makogon YF. Hydrates of Hydrocarbons. 1 ed. Tulsa, Oklahoma, USA: PennWell Publishing Company; 1997.
[13] Peng D-Y, Robinson DB. A new two-constant equation of state. Ind Eng Chem Fundam. 1976;15:59-64.
[14] Soave G. Equilibrium constants from a modified Redlich-Kwong equation of state. Chem Eng Sci. 1972;27:1197-203.
[15] Stryjek R, Vera JH. PRSV: An improved Peng—Robinson equation of state for pure compounds and mixtures. The canadian journal of chemical engineering. 1986;64:323-33.
[16] Wilson GM. Vapor-liquid equilibria, correlation by means of a modified Redlich-Kwong equation of state. Adv Cryog Eng: Springer; 1964. p. 168-76.
[17] Patel NC, Teja AS. A new cubic equation of state for fluids and fluid mixtures. Chem Eng Sci. 1982;37:463-73.
[18] Redlich O, Kwong JNS. On the thermodynamics of solutions. V. An equation of state. Fugacities of gaseous solutions. Chem Rev. 1949;44:233-44.
[19] Aspen HYSYS V10, AspenTech, Calgary 2020.
[20] Campestrini M. Thermodynamic study of solid-liquid-vapor equilibrium: application to cryogenics and air separation unit 2014.
[21] Baker CJ, Hughes TJ, Rowland D, Oakley J, Aman Z, Frotscher O, et al. ThermoFAST 1.3 Thermodynamics Calculator for Natual Gas Properties. Fluid Science and Resources, The University of Western Australia (https://www.fsr.ecm.uwa.edu.au/software/thermofast/); 2020.
[22] Baker CJ, Siahvashi A, Oakley JH, Hughes TJ, Rowland D, Huang S, et al. ThermoFAST: A new tool for predicting solids formation risk in cryogenic gas processing. 2018.
[23] Falloon PE, Baker CJ, May EF. ThermoFAST Web 0.4. (https://thermofastweb.azurewebsites.net/): Fluid Science and Resources research group, The University of Western Australia. ; 2021.

[24] Rowland D, Baker C, May EF. JESS: Cryogenic Solid Solubility (http://jess.murdoch.edu.au/cryobase.shtml). 2019.
[25] Rowland D, Baker C, May EF. Solubility of Heavy Hydrocarbons in Cryogenic Fluids. Tulsa, Oklahoma, USA: GPA Midstream Association; 2019. p. 69.
[26] Fonseca JMS, Dohrn R, Peper S. High-pressure fluid-phase equilibria: Experimental methods and systems investigated (2005 - 2008). Fluid Phase Equilib. 2011;300:1-69.
[27] Peper S, Fonseca JMS, Dohrn R. High-pressure fluid-phase equilibria: Trends, recent developments, and systems investigated (2009 - 2012). Fluid Phase Equilib. 2019;484:126-224.
[28] Coyle D, Vega F, Durr C. Natural gas specification challenges in the LNG industry. 15th international conference and exhibition on liquefied natural gas, Barcelona, Spain2007. p. 1-21.
[29] Pikaar MJ. A study of phase equilibria in hydrocarbon-CO2 systems. 1959.
[30] Sterner CJ. Phase Equilibria in the CO 2-Methane Systems. Adv Cryog Eng: Springer; 1961. p. 467-74.
[31] Cheung H, Zander EH. Solubility of carbon dioxide and hydrogen sulfide in liquid hydrocarbons at cryogenic temperatures. Chem Eng Progress Symposium Series1968. p. 34-43.
[32] Streich M. N2 removal from natural gas. Hydrocarbon Processing. 1970;49:86-&.
[33] Preston GT, Funk EW, Prausnitz JM. Solubilities of hydrocarbons and carbon dioxide in liquid methane and in liquid argon. J Phys Chem. 1971;75:2345-52.
[34] Kurata F. GPA RR-10: Solubility of Solid Carbon Dioxide in Pure Light Hydrocarbons and Mixtures of Light Hydrocarbons. Gas Processors Association; 1974.
[35] Agrawal GM, Laverman RJ. Phase behavior of the methane-carbon dioxide system in the solid-vapor region. Adv Cryog Eng: Springer; 1995. p. 327-38.
[36] Voss G. PhD thesis. Berlin: Technical University of Berlin, Rep. Knapp H.; Teller M.; Langhorst R. Solid-Liq. Equilib. Data Collect. Vol VIII Part 1 Chem. Data Ser. Dechema: Frankfurt am Main, 1987; 1975.
[37] Sparks KA, Sloan ED. GPA RR-71: Water Content of NGL in Presence of Hydrates. Gas Process Association; 1983.
[38] J. BG. Corporate Source: Shell Res Ltd Thornton Res Centre P O Box 1 Chester Rep Knapp H; Teller M; Langhorst R Solid-Liq Equilib Data Collect Vol VIII Part 1 Chem Data Ser Dechema: Frankfurt am Main, 1987. 1987.
[39] Le TT, Trebble MA. Measurement of carbon dioxide freezing in mixtures of methane, ethane, and nitrogen in the solid− vapor equilibrium region. J Chem Eng Data. 2007;52:683-6.
[40] Zhang L, Burgass R, Chapoy A, Tohidi B, Solbraa E. Measurement and modeling of CO2 frost points in the CO2–methane systems. J Chem Eng Data. 2011;56:2971-5.
[41] Gao T, Shen T, Lin W, Gu A, Ju Y. Experimental determination of CO2 solubility in liquid CH4/N2 mixtures at cryogenic temperatures. Ind Eng Chem Res. 2012;51:9403-8.
[42] Shen T, Gao T, Lin W, Gu A. Determination of CO2 solubility in saturated liquid CH4+ N2 and CH4+ C2H6 mixtures above atmospheric pressure. J Chem Eng Data. 2012;57:2296-303.
[43] Xiong X, Lin W, Jia R, Song Y, Gu A. Measurement and calculation of CO2 frost points in CH4+ CO2/CH4+ CO2+ N2/CH4+ CO2+ C2H6 mixtures at low temperatures. J Chem Eng Data. 2015;60:3077-86.
[44] Stringari P, Campestrini M, Rivera-Tinoco R. GPA RR-240: CO2 Freezing in Cryogenic Processes. Gas Processors Association; 2018.
[45] Neumann A, Mann R. Solubility of solid hydrocarbons and methanol in liquid methane. Kaltetechnik-Klimatisierung. 1970;22:182-3.
[46] Neumann A, Mann R, Von Szalghary WD. Solubility of solid benzene in liquid hydrocarbons. Kaeltetech Klim. 1972;24:145-9.
[47] Kuebler GP, McKinley C. Solubility of solid benzene, toluene, n-hexane, and n-heptane in liquid methane. Adv Cryog Eng: Springer; 1974. p. 320-6.
[48] Luks KD, Hottovy JD, Kohn JP. Three-phase solid-liquid-vapor equilibriums in the binary hydrocarbon systems methane-n-hexane and methane-benzene. J Chem Eng Data. 1981;26:402-3.
[49] Teller M, Knapp H. DETHERM database. 1985.
[50] Rijkers M, Malais M, Peters CJ, de Swaan Arons J. Experimental determination of the phase behavior of binary mixtures of methane+ benzene: Part I. Vapor+ liquid, solid benzene+ liquid,

solid benzene+ vapor and solid benzene+ liquid+ vapor equilibria. Fluid Phase Equilib. 1992;77:327-42.
[51] Hughes TJ, Kandil ME, Graham BF, Marsh KN, Huang SH, May EF. Phase equilibrium measurements of (methane+ benzene) and (methane+ methylbenzene) at temperatures from (188 to 348) K and pressures to 13 MPa. J Chem Thermodyn. 2015;85:141-7.
[52] Siahvashi A, Al Ghafri SZ, May EF. Solid-Fluid Equilibrium Measurements of Benzene in Methane and Implications for Freeze-out at LNG Conditions. Fluid Phase Equilib. 2020;519.
[53] Kurata F. GPA RR-14: solubility of heavier hydrocarbons in liquid methane. Gas Processors Association; 1975.
[54] Luks KD, Kohn JP, Liu PH, Kulkarni AA. Solubility of hydrocarbons in cryogenic NGL and LNG. Hydrocarbon Process;(United States). 1975;54.
[55] Morlet J. The density and miscibility of liquefied hydrocarbon gases at low temperatures. Rev Inst Fr Pet. 1963;18:127-43.
[56] Kuebler GP, McKinley G. Solubility of solid n-butane and n-pentane in liquid methane. In: Timmerhaus KD, Weitzel DH, editors. Adv Cryog Eng. Boston WA, US: Springer; 1976. p. 509-15.
[57] Brew TCL. A study on the solubility of heavy hydrocarbons in liquid methane and methane containing mixtures: University of Ottawa (Canada); 1977.
[58] J. BG. Corporate Source: Shell Res Ltd Thornton Res Centre P O Box 1 Chester Rep DECHEMA 1973 1973.
[59] Dickinson E, Knobler CM, Scott RL. Solid/liquid phase equilibria in the mixtures methane+ n-hexane and methane+ n-pentane. Journal of the Chemical Society, Faraday Transactions 1: Physical Chemistry in Condensed Phases. 1973;69:2179-87.
[60] Baughman GL, Gl B, Sp W, Dd D. The solid+ vapor phase equilibrium and the interaction second virial coefficients for argon+, nitrogen+, methane+, and helium+ neopentane. 1974.
[61] Siahvashi A, Ghafri SZSA, Yang X, Rowland D, May EF. Solubility of Neopentane in Methane at Cryogenic Conditions with Implications for LNG Production. 2020:(summited to Energy).
[62] Beck LA. Solubility, density, and freezing point data for solutions of methane in n-hexane: University of Kansas, Chemical Engineering; 1956.
[63] Shim J, Kohn JP. Multiphase and Volumetric Equilibria of Methane-n-Hexane Binary System at Temperatures Between-110° and 150° C. J Chem Eng Data. 1962;7:3-8.
[64] de Mateo A, Kurata F. Correlation and prediction of solubilities of solid hydrocarbons in liquid methane using the Redlich-Kwong equation of state. Industrial & Engineering Chemistry Process Design and Development. 1975;14:137-40.
[65] Kohn JP, Luks KD. GPA RR-22: Solubility of Hydrocarbons in Cryogenic LNG and NGL Mixtures. Gas Processors Association; 1977.
[66] Tiffin DL, Luks KD, Kohn JP. Solubility enhancement of solid hydrocarbons in liquid methane due to the presence of ethane. Adv Cryog Eng: Springer; 1978. p. 538-43.
[67] Kohn JP, Luks KD, Liu PH, Tiffin DL. Three-phase solid-liquid-vapor equilibriums of the binary hydrocarbon systems methane-n-octane and methane-cyclohexane. J Chem Eng Data. 1977;22:419-21.
[68] Jasperson LV, McDougal RJ, Wilson GM. Equilibrium Data (SLE and VLE) for Heavy and Light Hydrocarbons at Cryogenic Temperatures. Wiltec Research Co., Inc., Provo, Utah, GPA RR-215 Project; 2014.
[69] Lemmon EW, Bell IH, Huber ML, McLinden MO. NIST Standard Reference Database 23: Reference Fluid Thermodynamic and Transport Properties-REFPROP, Version 10.0, National Institute of Standards and Technology, 2018. URL http://wwwnistgov/srd/nist23cfm.
[70] Rowley RL, Wilding WV, Oscarson JL, Yang Y, Zundel NA, Daubert TE, et al. Design Institute for Physical Properties (DIPPR) 801 Database. AICHE: https://app.knovel.com/web/toc.v/cid:kpDIPPRPF7/; 2018.
[71] InfoChem KBC Advanced Technologies PLC. MultiFlash 6.2. 2019.
[72] Prausnitz JM, Lichtenthaler RN, De Azevedo EG. Molecular thermodynamics of fluid-phase equilibria: Pearson Education; 1998.

[73] Parks GS, Huffman HM, Thomas SB. THERMAL DATA ON ORGANIC COMPOUNDS. VI. THE HEAT CAPACITIES, ENTROPIES AND FREE ENERGIES OF SOME SATURATED, NON-BENZENOID HYDROCARBONS1. JACS. 1930;52:1032-41.
[74] Moysan JM, Huron MJ, Paradowski H, Vidal J. Prediction of the solubility of hydrogen in hydrocarbon solvents through cubic equations of state. Chem Eng Sci. 1983;38:1085-92.
[75] Voros NG, Tassios DP. Vapor-liquid equilibria in nonpolar/weakly polar systems with different types of mixing rules. Fluid Phase Equilib. 1993;91:1-29.